Intramolecular circuits connected to N electrodes using a scattering matrix approach

S. Ami and C. Joachim

Centre d'Elaboration de Materiaux et d'Etudes Structurales,

CNRS-UPR8011, 29 rue Jeanne Marvig, Boîte Postale 4347, 31055 Toulouse Cedex 4, France

(Received 26 July 2001; revised manuscript received 26 November 2001; published 3 April 2002)

The scattering matrix technique is extended to describe the electronic transport characteristics of intramolecular circuits driven in a ballistic or a tunnel transport regime. The circuit is assumed to be connected by N electrodes. As a working example, the electronic properties of a T-node circuit are presented leading to the design of an OR logic gate working in a ballistic regime. In the tunnel regime, only the "node" Kirchhoff law of circuit remains valid at the nodes of an intramolecular tunnel circuit and the electronic characteristics of the branches composing the circuit are mutually independent. It results in a difficult design of a logic OR intramolecular gate of high performance and stability, pointing out the urge for new architectures to implement complex logic functions inside a single molecule.

I. INTRODUCTION

The goal of making a computing machine with molecule(s) has now taken many technological routes from molecular material[1] to quantum computing.[2] Between these two extreme cases stands molecular electronics in its hybrid or monomolecular version.[3] Hybrid devices such as molecular rectifiers have long been proposed.[4] Molecular switches,[5] amplifiers,[6] and transistors[7–9] have now been experimented. This opens ways for the design of complex hybrid molecular circuits[10–12] where the molecular devices are interconnected by metallic wires.

At the opposite, monomolecular electronics uses monomolecular circuits. A monomolecular circuit is an assemblage of molecular functional groups covalently bonded together resulting in a single supermolecule per circuit. A functional group is, for example, a molecular wire or an intramolecular switch. Compared to a molecular switch operating in a hybrid molecular circuit, an intramolecular switch is switched "on" and "off" by a signal coming from another part of the supermolecule with no reference to external electrodes. The information inside a monomolecular circuit is carried outside by a quantum exchange of electrons between the different molecular functional groups of the corresponding supermolecule. Such versions of molecular electronics have also long been proposed.[13]

In this intramolecular approach and up to now, only molecular wires have been accessible to experiments.[14] One reason is the difficulty of interconnecting a single, large molecule equipped with many interconnecting groups to more than two metallic electrodes. The second reason is the absence of rules for the design of an intramolecular circuit in a single supermolecule.[15] Chemists know how to synthesize molecules more complicated than a molecular wire.[16] But the expected intrinsic properties of such molecules remain based on the analogy, for example, between the shape of a three-branch molecule and of a three-terminal solid-state device. No detailed calculations of electron transport phenomenon through a fully interconnected multibranched molecule exist.

To establish intramolecular circuit design rules, we propose here an extension of our elastic-scattering quantum chemistry (ESQC) technique.[17] Our final goal is the integration of the full circuit of a computer inside a single supermolecule without the use of mesoscopic or nanoscopic metallic wiring to interconnect the switching molecular group operating in this intramolecular circuit. In the following, the supermolecule is assumed to be connected to N metallic electrodes, the purpose of which is to feed electrons in and out.

When the electronic transport regime in the circuit is a tunnel transport regime,[3] the electronic functionalities of an intramolecular circuit can be described by a scattering matrix S when they are characterized from the electrodes. Our extension of ESQC is based on a multichannel scattering approach, already applied to mesoscopic devices.[18,19] This approach was proved to be essential to predict the in and out ballistic current intensity, where the scattering matrix elements depend on the topology of the circuits (linear, loops, nodes), on the number of interconnects[20] and on the magnetic or electric field applied.[21] As for mesoscopic circuits, the S matrix for an intramolecular circuit depends on the topology of the circuit. But it also depends on the detailed chemical structure of its molecular branches and nodes.

To simplify the description of our calculation technique, we present here a tight-binding version of this N-electrode extension of ESQC (N-ESQC). This has the advantage of minimizing the number of electronic states per atom of the intramolecular circuit and of the metallic interconnects. Furthermore, a simple adjustment of parameters tunes the transport regime inside the molecular circuit from a ballistic to a tunneling regime. The generalization of N-ESQC to the extended Huckel molecular orbital (EHMO) semiempirical technique including many orbitals per atom is mathematically straightforward but technically more demanding.

In Sec. II, the technique for calculating the scattering matrix of a general intramolecular circuit with N interconnects is presented. Section III discusses the properties of a three-port intramolecular node in a ballistic transport regime. Standard properties of a waveguide splitter are recovered together with those of a symmetric node for use in complex electronic ballistic circuits. These scattering calculations are also applied to the design of a monolithic OR logic gate in a ballistic regime, an example that requires a fine adjustment of the circuit tight-binding structure. Section IV presents a gener-
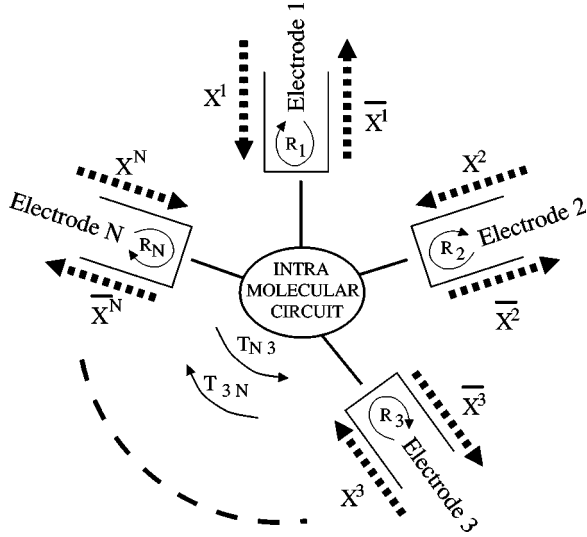
FIG. 1. Definition of the multiple incoming and outgoing electronic Bloch wave amplitudes on an intramolecular circuit connected to N metallic electrodes.
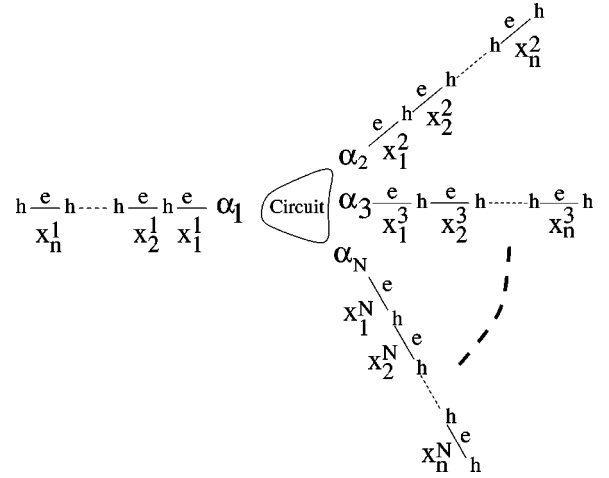

FIG. 2. A simplified tight-binding version of the N-electrodes circuit presented in Fig. 1. Each atom of the electrodes is described by one orbital and the details of the central circuit are specified in Secs. III and IV, depending on its functionality.

alization of the results to the tunneling regime of transport for a three-port intramolecular circuit in a star configuration. In electrical engineering, the description of the electric properties of such a three-port circuit requires the two "node" and "mesh" Kirchhoff laws.[22] We demonstrate that only the "node" law remains valid in the tunneling regime. In Sec. V, the extension of this work to the chemical optimization of passive intramolecular circuits is discussed.

For the N-port circuit presented in Fig. 1, the $S = [S_{ij}]$ scattering matrix description of its electronic transport properties measured from N metallic electrodes interconnected to the sources and the sinks is defined by[23]

$$
\begin{bmatrix} \overline{X^1} \\ \overline{X^2} \\ \vdots \\ \overline{X^N} \end{bmatrix} = \begin{pmatrix} S_{11} & S_{12} & \cdots & S_{1N} \\ S_{21} & S_{22} & \cdots & S_{2N} \\ \vdots & \vdots & \ddots & \vdots \\ S_{N1} & S_{N2} & \cdots & S_{NN} \end{pmatrix} \begin{bmatrix} X^1 \\ X^2 \\ \vdots \\ X^N \end{bmatrix}, \quad (1)
$$

where the $(X^m, \overline{X^m})$ are the respective incoming and outgoing amplitudes of the Bloch electronic wave used to test the scattering properties of the central intramolecular circuit (Fig. 1) from a given electrode m. The transmission coefficient from electrode m to electrode n is defined by $T_{mn} = \overline{X^n}/X^m|_{Xj=0, \, j \neq m} = \|S_{nm}\|^2$ and the reflection coefficient on electrode m by $R_m = \overline{X^m}/X^m|_{Xj=0, j \neq m} = \|S_{mm}\|^2$.

II. CALCULATION OF THE SCATTERING MATRIX

We consider the complete tight-binding electronic circuit presented in Fig. 2 consisting of N electrodes connected to a central intramolecular circuit. The electronic structure of each electrode is described by a semi-infinite one-dimensional chain of identical atoms. Each atom of a given electrode k is described by a single electronic state $|s_n^k\rangle$, $k \in [1,N]$, of energy e, interacting with the other states of the same chain in a nearest-neighbor approximation with an

electronic interaction energy h. Each electrode is described by a half filled conduction band with no gap at the Fermi level e.

This central circuit is also described in a tight-binding approximation by a set of L electronic states $|s_i^0\rangle$, $i \in [1,L]$ with the corresponding state energy ω_i, whatever the topology of the circuit. This circuit is connected to the electrodes via a simple electronic coupling α_i per chain.

The total electronic Hamiltonian of the tight-binding system of Fig. 2 is given by

$$
\mathcal{H} = \sum_{n=1}^{+\infty} \sum_{k=1}^{N} h(|s_n^k\rangle\langle s_{n+1}^k| + |s_{n+1}^k\rangle\langle s_n^k|) + e|s_n^k\rangle\langle s_n^k|
$$

$$
+ H_{Circuit} + H_{Circuit-electrode}, \quad (2)
$$

where the first term describes the electronic structure of the N electrodes interconnecting the central circuit to external sources and ground. The second term $H_{Circuit}$ of Eq. (2) describes the electronic structure of the central circuit, which can be of any topology and structure so long as its number of states L remains finite in any direction. The last term $H_{Circuit-electrode}$ of Eq. (2) is the Hamiltonian describing the electronic interaction between this circuit and the N electrodes. It can simply describe finite tight-binding chains of the same structure as the electrodes. It can also introduce the specific band structure of N molecular wires, interconnecting the central circuit to the N external metallic electrodes (see Sec. IV).

The wave function $|\psi\rangle$ of the entire circuit of Fig. 2 is a solution of the eigenvalue problem: $\mathcal{H}|\psi\rangle = E|\psi\rangle$ where $|\psi\rangle$ can be decomposed on the basis set $\{|s_n^k\rangle, |s_i^0\rangle\}$,

$$
|\psi\rangle = \sum_i d_i |s_i^0\rangle + \sum_{n>0} \sum_{k=1}^{N} x_n^k |s_n^k\rangle. \quad (3)
$$

The electronic transmission properties of the central circuit viewed from the N electrodes are recovered by substi-

tuting Eq. (3) in the eigenvalue problem while $\mathcal{H}$ is given by Eq. (2). As usual,[17] projecting this equation on the state subspace spanned by the N electrodes states $|s_n^k\rangle$ for $n>1$ leads to a set of second-order difference equations, one subset for each electrode:

$$h x_{n+1}^k + e x_n^k + h x_{n-1}^k = E x_n^k, \quad n>1, \quad k \in [1,N]. \quad (4)$$

For a given electrode k, such a subset of equations can be rewritten in the transfer-matrix form[17]

$$\begin{pmatrix} x_{n-1}^k \\ x_n^k \end{pmatrix} = \begin{bmatrix} \dfrac{E-e}{h} & -1 \\ 1 & 0 \end{bmatrix} \begin{pmatrix} x_n^k \\ x_{n+1}^k \end{pmatrix} = P \begin{pmatrix} x_n^k \\ x_{n+1}^k \end{pmatrix} \quad \text{for } n>1.$$

P is the so-called spatial propagator along a given tight-binding chain away from the central tiny circuit. For the full set of N electrodes and by adopting the more compact notation

$$\mathcal{X}_n^k = \begin{pmatrix} x_n^k \\ x_{n+1}^k \end{pmatrix},$$

we have

$$\begin{cases} \mathcal{X}_{n-1}^1 = P \mathcal{X}_n^1 \\ \vdots \\ \mathcal{X}_{n-1}^N = P \mathcal{X}_n^N \end{cases} \quad \text{and} \quad \mathcal{X}_1^k = P^{n-1} \mathcal{X}_n^k \quad \text{with } k \in [1,N]. \quad (5)$$

For each tight-binding chain, it is known that there are nonpropagative and propagative eigensolutions, characterized, respectively, by the real or the modulus-one complex eigenvalues of the spatial propagator P.[17] On a given electrode k and for an incident electron of energy E chosen such that $|E-e|<2|h|$, the two propagative modes are given by the two conjugate eigenvalues of P: $e^{+i\theta}, e^{-i\theta}$ corresponding to the dispersion relation $E = e + 2h \cos \theta$. Therefore, for a given electrode k[17]

$$\mathcal{X}_n^k = U_{n,n+1} \begin{bmatrix} \overline{X^k} \\ X^k \end{bmatrix}, \quad (6)$$

where X^k and $\overline{X^k}$ are the amplitudes of the incoming and outgoing electronic waves on the electrode k as defined in Fig. 1, with

$$U_{n,n+1} = \begin{bmatrix} e^{in\theta} & e^{-in\theta} \\ e^{i(n+1)\theta} & e^{-i(n+1)\theta} \end{bmatrix}.$$

Since $P U_{n,n+1} = U_{n-1,n}$, then for any electrode

$$\mathcal{X}_1^k = U_{1,2} \begin{bmatrix} \overline{X^k} \\ X^k \end{bmatrix}. \quad (7)$$

After using the propagator technique to describe the transmission properties of a given electrode, the interactions between all these electrodes through the central circuit are now considered. For this purpose, the eigenvalue problem $\mathcal{H}|\psi\rangle$

$= E|\psi\rangle$ is now projected on the Hilbert subspace spanned by the states $|s_i^0\rangle i \in [1,L]$ and $|s_1^k\rangle k \in [1,N]$. A finite set of $(L+N)$ second-order difference equations results, which can be separated into 2 subsets. One subset of L equations determines the probability amplitudes d_l on the central circuit as a function of the probability amplitude vector $\mathcal{X}_1^k$ found at the end state of a given electrode. It can be rewritten in the matrix form

$$C \begin{bmatrix} d_1 \\ d_2 \\ \vdots \\ d_l \end{bmatrix} + MQ \begin{bmatrix} \mathcal{X}_1^1 \\ \vdots \\ \mathcal{X}_1^N \end{bmatrix} = 0, \quad (8)$$

with

$$C = \begin{bmatrix} (\omega_1 - E) & & & \text{internal} \\ & (\omega_2 - E) & & \text{circuit-coupling} \\ \text{internal} & & \ddots & \\ \text{circuit-coupling} & & & (\omega_l - E) \end{bmatrix}.$$

In its tight-binding form, the matrix C accounts for the central circuit electronic structure including the circuit topology, atomic level energy, and the interatomic electronic interactions. $M(l,k) = \langle s_l^0 | \mathcal{H} | s_1^k \rangle$ is a (L,N) rectangular matrix giving the electronic coupling between the end state of each electrode and the first external frontier state of the central circuit. Q is a rectangular $(N,2N)$ matrix. It takes into account the fact that, in the set of L equations (the internal part of the circuit), only the $|s_1^k\rangle$ amplitudes have to be considered. This matrix is defined by $Q(i,j) = \delta_{j,2i-1}$ with $i \in [1,N]$ and $j \in [1,2N]$.

The second subset of N equations determines the probability amplitude on each of the end electrode states $|s_1^k\rangle$, which depends on the external frontier states of the internal circuit in the nearest-neighbor approximation. From this second subset, the $[d_i]$ and $[\mathcal{X}_1^k]$ vectors are related by the simple equation

$$\begin{bmatrix} (e-E) & h & 0 & \cdots & \cdots & 0 \\ \vdots & \vdots & \ddots & \ddots & \vdots & \vdots \\ 0 & \cdots & \cdots & 0 & (e-E) & h \end{bmatrix} \begin{bmatrix} \mathcal{X}_1^1 \\ \vdots \\ \mathcal{X}_1^N \end{bmatrix}$$
$$+ {}^t M \begin{bmatrix} d_1 \\ d_2 \\ \vdots \\ d_l \end{bmatrix} = 0. \quad (9)$$

Equations (8) and (9) form a homogeneous system of equations for the unknown vectors $[d_i]$ and $[\mathcal{X}_1^k]$. But the d_i are not explicitly required to calculate the electronic transmission properties of the central circuit and so, as in the effective Hamiltonian technique used in ESQC,[15] the d_i amplitudes are eliminated from Eqs. (8) and (9) leading to the following equation:

$$
\left(\begin{bmatrix} (e-E) & h & 0 & \cdots & \cdots & 0 \\ 0 & \vdots & \ddots & \ddots & \vdots & \vdots \\ \vdots & \vdots & \ddots & \ddots & \vdots & 0 \\ 0 & \cdots & \cdots & 0 & (e-E) & h \end{bmatrix}\right.
$$

$$
\left. -\,{}^t M C^{-1} M Q \right) \begin{bmatrix} \mathcal{X}_1^1 \\ \vdots \\ \mathcal{X}_1^N \end{bmatrix} = 0. \tag{10}
$$

Substituting Eq. (7) in Eq. (10) for each interconnection, we obtain N relations between the $2N$ amplitudes $\{X^1, \overline{X^1}, \ldots, X^m, \overline{X^m}\}$:

$$
\begin{bmatrix} \epsilon_1 - E & h & \Gamma_{12} & 0 & \cdots & \Gamma_{1N} & 0 \\ \Gamma_{12} & 0 & \epsilon_2 - E & h & \cdots & \Gamma_{2N} & 0 \\ \vdots & \vdots & \ddots & \ddots & \ddots & \vdots & \vdots \\ \Gamma_{1N} & 0 & \cdots & \Gamma_{N-1N} & 0 & \epsilon_N - E & h \end{bmatrix}
$$

$$
\times \begin{bmatrix} [U_{1,2}] & & & 0 \\ & [U_{1,2}] & & \\ & & \ddots & \\ 0 & & & [U_{1,2}] \end{bmatrix} \begin{bmatrix} \overline{X^1} \\ X^1 \\ \overline{X^2} \\ X^2 \\ \vdots \\ \overline{X^N} \\ X^N \end{bmatrix} = 0. \tag{11}
$$

The Γ_{ij}, $(i,j) \in [1,N]^2$ are the effective electronic couplings between two given electrodes through the central circuit. They depend on the C matrix elements. The ϵ_i are the effective energy levels of the end states of the chains defined by their interaction with the central circuit. From Eq. (11), algebraic manipulation gives directly the S scattering matrix, i.e., the relation between $\{\overline{X^1}, \ldots, \overline{X^N}\}$ and $\{X^1, \ldots, X^N\}$.

III. SIMPLE CIRCUIT IN THE BALLISTIC TRANSPORT REGIME

As a first example, we consider the three-port circuit presented in Fig. 3 consisting of three wires A, B, and C feeding a central circuit composed of a simple single state $|s_1^0\rangle$. This central state is coupled to one chain by an electronic interaction δ and to the two other chains by the interactions γ and α. The electronic coupling β was added to include a direct interaction between electrodes B and C without passing through the central state. Because there is no electronic gap in the band structure of the tight-binding chain describing the wires, this circuit is the tight-binding version of three-port metallic circuits often considered in mesoscopic physics.[23] The difference between those and our tight-binding description is that the interaction between each chain can be tuned independently. Furthermore, the central electronic state energy ω can be shifted to compensate for a variation of those interactions in order to tune all the transmission or reflection coefficients of this three-port circuit.

Using Eq. (11), and after some algebraic manipulations, the general analytic expression for the scattering matrix $S(E)$ of this simple circuit is given by

$$
S(E) = -\exp(-2i\theta) \begin{bmatrix} \epsilon_A - E + he^{i\theta} & \Gamma_{AB} & \Gamma_{AC} \\ \Gamma_{AB} & \epsilon_B - E + he^{i\theta} & \Gamma_{BC} \\ \Gamma_{AC} & \Gamma_{BC} & \epsilon_C - E + he^{i\theta} \end{bmatrix}^{-1} \begin{bmatrix} \epsilon_A - E + he^{-i\theta} & \Gamma_{AB} & \Gamma_{AC} \\ \Gamma_{AB} & \epsilon_B - E + he^{-i\theta} & \Gamma_{BC} \\ \Gamma_{AC} & \Gamma_{BC} & \epsilon_C - E + he^{-i\theta} \end{bmatrix}. \tag{12}
$$

S is energy dependent but satisfies the usual $SS^\dagger = I$ identity with $E = e + 2h\cos\theta$. The effective energies $\epsilon_X(E)$ with $X = A$, B, or C and the effective interactions $\Gamma_{XY}(E)$ with $X,Y = A$, B, or C appearing in Eq. (12) are specified in the following, depending on the exact function performed by the circuit of Fig. 3. They are calculated using the energy-dependent effective Hamiltonian technique as used in the ESQC technique and already applied to simple tight-binding two electrode systems.[17] For example, with $\beta = 0$, $\alpha = \gamma = h$, and $\omega = e$, the effective interactions are given directly by $\Gamma_{BC}(E) = h^2/(E-e)$, $\Gamma_{AB}(E) = \Gamma_{AC}(E) = \delta h/(E-e)$ and the effective energies by $\epsilon_A(E) = e + \delta^2/(E-e)$ and $\epsilon_B(E) = \epsilon_C(E) = e + h^2/(E-e)$. In this case and for $E = e$, all the matrix elements of $S(E)$ are real valued and the $S(E=e)$ matrix becomes, using Eq. (12),

$$
S = \begin{pmatrix} x & \sqrt{\varepsilon} & \sqrt{\varepsilon} \\ \sqrt{\varepsilon} & a & b \\ \sqrt{\varepsilon} & b & a \end{pmatrix}, \tag{13}
$$

with $\sqrt{\varepsilon} = 2\delta/(2+\delta^2)$, $a = -\delta^2/(2+\delta^2)$, $b = 2/(2+\delta^2)$, and $x = -(a+b)$. This is exactly the same as the scattering matrix of the three-port circuit used by Buttiker[24] with $T_{AB}(E=e) = T_{AC}(E=e) = \varepsilon$. It describes the electronic scattering properties of a mesoscopic metallic loop accessible in a ballistic transport regime via a T node using a single metallic wire playing the role of a single entrance port.[24] But for $E \neq e$, the $S(E)$ matrix elements are complex valued and the simple expression (13) no longer holds as already demonstrated in Ref. 25.
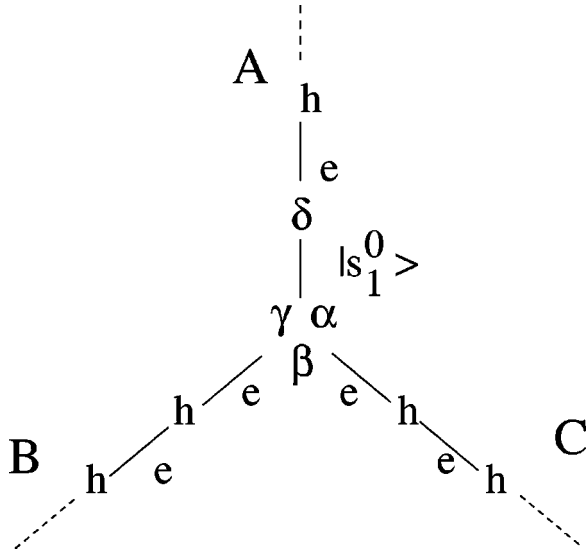
FIG. 3. The tight-binding implementation of a three-port T-like circuit including one central electronic state $|s_i^0\rangle$ and three connections represented by three semi-infinite chains A, B, and C.

This simple example illustrates how our general S-matrix approach can handle well known and simple examples of ballistic circuits already considered in the literature through the Green's-function approach.[19] For our purpose, to calculate large intramolecular circuits using a quantum chemistry approach, the S matrix is preferable as already demonstrated in our EHMO-ESQC approach in the case of two electrodes.[34] The parameters $\delta, \omega, \alpha, \beta, \gamma$ controlling the scattering properties of the circuit (Fig. 3) can be optimized for two different purposes. The first is the realization of a Bloch waveguide splitter. In this case, and choosing electrode A for the input electrode of the splitter, the controlling parameters are chosen for the transmission coefficients T_{AB} and T_{AC} to be equal. Furthermore, a full splitter is obtained when $R_A = 0$.

The second function that the three-port circuit of Fig. 3 can perform is to be a generic symmetric node for its use in complex and monolithic ballistic circuits made of many others nodes of the same type. In this case, all the transmission coefficients and all the reflection coefficients must be respectively equal whatever the electrodes for the input and the output. These two functions are discussed in the following sections using a general property of the scattering matrix (12):

$$\frac{S_{2,1}}{S_{3,1}} = \frac{E\Gamma_{AB} + \Gamma_{AC}\Gamma_{BC} - \epsilon_A \Gamma_{AB} - h\Gamma_{AB}\exp(-i\theta)}{E\Gamma_{AC} + \Gamma_{AB}\Gamma_{BC} - \epsilon_B \Gamma_{AC} - h\Gamma_{AC}\exp(-i\theta)}. \tag{14}$$

As a function of the electron incident energy E defined in the A electrode, this ratio measures the electronic transparency equilibration between the chain A and B and between A and C when the central node is connecting A to B and C. It holds also for the ratio of the other matrix elements $[S_{ij}]$ after a circular permutation of the input and the output branches. The ratio (14) is easily converted to the transmission ratio T_{AB}/T_{AC} between the A-B and the A-C branches:
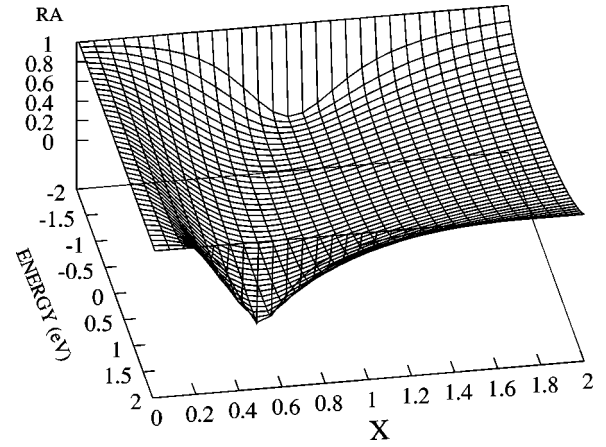

FIG. 4. Reflection coefficient on the input electrode A as a function of the energy of the incident electron and of the value of the coupling parameter defining the node for $X = \alpha = \beta = \gamma$ in eV. The energy scale is relative to e and the resonant integral along the electrodes is $h = 1$ eV.

$$\frac{T_{AB}}{T_{AC}} = \left(\frac{\Gamma_{AB}}{\Gamma_{AC}}\right)^2 \frac{(e-E)\mathcal{A} + h^2 + \mathcal{A}^2}{(e-E)\mathcal{B} + h^2 + \mathcal{B}^2}, \tag{15}$$

with $\mathcal{A} = E + \Gamma_{AC}\Gamma_{BC}/\Gamma_{AB} - \epsilon_C$ and $\mathcal{B} = E + \Gamma_{AB}\Gamma_{BC}/\Gamma_{AC} - \epsilon_B$.

A. The waveguide splitter

Setting A as the input electrode, a simple splitter is obtained by choosing $\delta = h$ and $\omega = e$. The condition $\delta = h$ introduces a coupling between A and the two output chains, which respects the periodic structures of the chains from A to B and from A to C. The condition $\omega = e$ suppresses the possibility of a reflection along A, which is always introduced by a nonresonant state.[17] With such a parameter choice, we have in Eq. (12), $\Gamma_{AB} = \alpha$, $\Gamma_{AC} = \gamma$, $\Gamma_{BC} = \beta$, and $\epsilon_A = \epsilon_B = \epsilon_C = e$. In this case and for $\beta = \pm h$ or $\alpha = \pm \gamma$, the ratio T_{AB}/T_{AC} is equal to unity and a good symmetric splitter results for $\alpha = \beta = \gamma$. The transmitted Bloch wave is divided into two equal amplitudes. But this parameter adjustment does not provide a perfect splitter because the reflection coefficient R_A is not zero on electrode A. Furthermore, the optimum value of the coupling parameters to reach the minimum possible value $1/9$ for R_A (see below) varies as a function of the incident electron energy as indicated in Fig. 4.

With the circuit of Fig. 3, a full splitter is obtained only when $\beta = 0$ because, viewed from the input electrode A, a $\beta \neq 0$ coupling destroys the regularity of the electronic structure from A to B and from A to C. This regularity breakdown cannot be compensated by a fine adjustment of α and γ. When $\beta = 0$, the T_{AB}/T_{AC} ratio is simply given from Eq. (15) by

$$\frac{T_{AB}}{T_{AC}} = \left(\frac{\alpha}{\gamma}\right)^2. \tag{16}$$

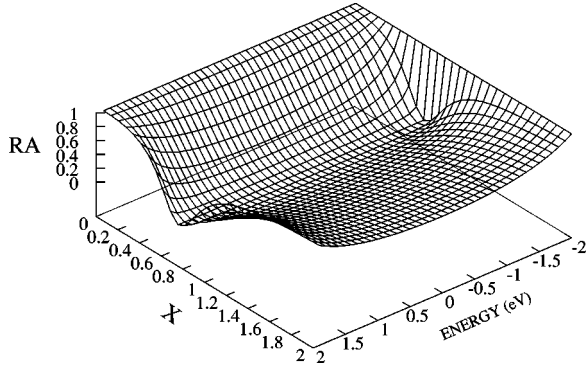Furthermore, the necessary and sufficient condition for $R_A = 0$ is given by the equation

FIG. 5. Reflection coefficient on input electrode A as a function of the energy of the incident electron and of the value of the coupling parameter for $X = \alpha = \gamma$ in eV and $\beta = 0$. The energy is relative to e and $h = 1$ eV.

$$(E - \omega)[e - E + h\exp(-i\theta)][e - E + h\exp(+i\theta)]$$
$$+ \delta^2[e - E + h\exp(-i\theta)]$$
$$+ (\gamma^2 + \alpha^2)[e - E + h\exp(+i\theta)] = 0 \quad \text{with} \quad \delta, \alpha, \gamma \neq 0,$$
$$(17)$$

which leads for $\omega = e$ to the solution $\alpha = \pm h/\sqrt{2}$, $\gamma = \pm h/\sqrt{2}$ and $\delta = h$ for all $E = e + 2h\cos\theta$. In Fig. 5 we present the variation of R_A as a function of E for different values of α and γ in the symmetric case. Depending on the sign chosen for α and γ, the two outputs of the splitter can be in phase or out of phase. The differences between the case $\beta \neq 0$ (Fig. 4) and $\beta = 0$ (Fig. 5) is that for $\beta = 0$, there exists a value $\alpha = \gamma$ value of which $R_A = 0$ independently of the incident energy of the electron (Fig. 5). When $\beta \neq 0$, the minimum R_A valley is not parallel to the energy axis as shown in Fig. 4.

B. The symmetric node for a ballistic circuit

It is more difficult to optimize the circuit parameters of Fig. 3 to obtain a generic symmetric node to be used in the design of ballistic circuits. Keeping the architecture of the circuit in Fig. 3, one solution is to choose again $\beta = 0$ and $\omega = e$ with $\alpha = \delta = \gamma$. In this case, and for all the E values, all the T_{AB}/T_{AC}, T_{BA}/T_{BC}, and T_{CA}/T_{CB} are equal to unity. Whatever the input electrode, the general expression for the reflection coefficient R from any input electrode is given by

$$R = \frac{C + \alpha^4[2(E - e)^2 + h^2]}{C + 9\alpha^4 h^2}, \quad (18)$$

with $C = h^2(E - \omega)[h^2(E - \omega) - 3\alpha^2(E - e)]$.

As presented in Fig. 6, the minimum value of Eq. (18), $R = 1/9$, is obtained for $\alpha = \sqrt{2/3}$ for all energies of the bands of the electrodes.

In the case of a multiple node interconnecting N electrodes instead of three and with these electrodes coupled together in the center with the same electronic interaction, a straightforward generalization of the preceding result shows that the optimized coupling to get a minimum reflection on
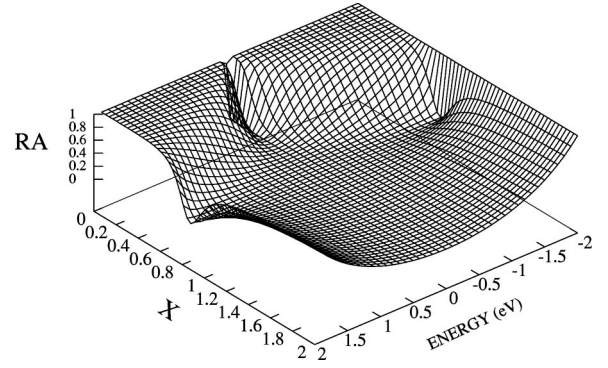
the node is $\alpha = \sqrt{2(E - \omega)/N(E - e)}$. In this case, the total reflection on the input electrode becomes $R = (1 - 2/N)^2$. As a consequence, we recover the well-know property in microwave circuits that the efficiency of a N node in its ability to transmit a wave from the input electrode to all the others decreases rapidly with the increase in the number N of the connected electrodes to which the input wave has to be distributed.

As presented in Fig. 7, to build a more efficient three-port node circuit, one may consider using a triangular circuit in the center made of three intermediate states instead of no states. Unfortunately, in the ballistic regime of transport, such a triangular circuit introduces a phase shift between the two paths of a Bloch wave passing from one electrode to another via the triangle. One path through the triangle is defined using one state of this central triangle and the other path using two states. This triangular circuit is therefore an interferometer with the phase shift per path defined by the values of the ω_i and of α, β, and γ.

The scattering characteristics of this triangular interferometer were calculated using the scattering matrix (12) with the

FIG. 6. Reflection coefficient on the input electrode A as a function of the energy of the incident electron relative to e and of the value of the coupling parameter for $X = \alpha = \delta = \gamma$ in eV and $h = 1$ eV.
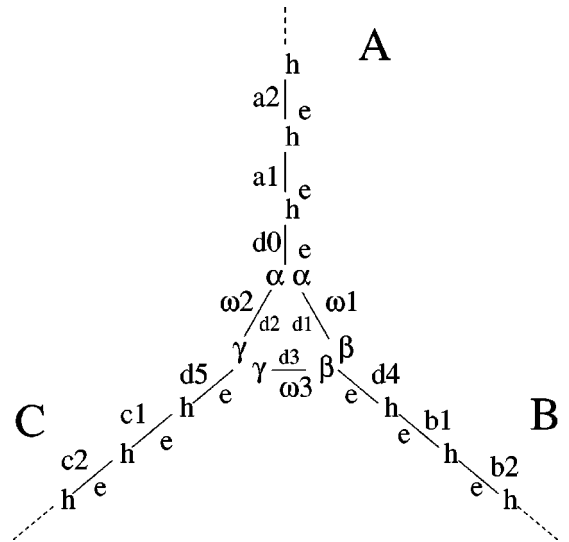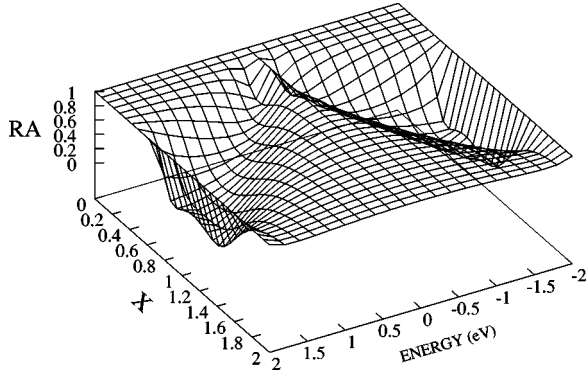

FIG. 7. A tight-binding design of a triangular three-port node made of three electronic states.

FIG. 8. Reflection coefficient on the input electrode A as a function of the energy of the incident electron relative to e and of the value of the coupling parameters for $X = \alpha = \beta = \gamma$ in eV, $h = 1$ eV and $\omega_1 = \omega_2 = \omega_3 = e$.

effective couplings and energies calculated using the effective Hamiltonian technique as described previously in this paper. The expression for those couplings and energies are no longer analytic because the corresponding discriminant for the inversion of the central Hamiltonian matrix is now of order 6. As presented in Fig. 8, a minimum of reflection is obtained for specific values of the incident energy and coupling parameters. But unlike the simple preceding three-port node, this is not valid for the entire energy range. On the $R_A(X,E)$ plot (Fig. 8), the valley of minimum R_A no longer exists unlike the case of Figs. 4, 5, 6 because for $E = 0$, the tight-binding circuit (Fig. 7) presents a total reflection. Furthermore, for the Fig. 7 circuit to be a symmetric node, the conditions $\alpha = \beta = \gamma$ must be respected, which preclude any finetuning of the corresponding reflection coefficients even by changing the ω_i.

C. An OR logic gate in the ballistic regime

To show the ability of our N-electrodes scattering approach to deal with more complex central circuits than a three-port node, we have designed an OR logic gate operating in a ballistic transport regime. The circuit presented in Fig. 9 is based on a resistance diode logic (RDL) design.[26] Notice

that such a design is normally restricted to electronic circuits working in a diffusive transport regime. Our circuit uses two tunnel rectifiers interconnected via finite length tight-binding chains to a central three-port node. The coupling coefficients γ between the node and those chains have been chosen to conform to the optimization discussed in Secs. III A and III B There is no defect along those chains and they have the same electronic structure as the chains representing the electrodes A, B, and C. This circuit can be considered as a simple model of a Y-shaped single wall carbon nanotube ballistic logic gate.[27] In such a Y macromolecule, a single kink made of pentagonal and heptagonal defects in one branch will act as an intramolecular tunnel rectifier.[28]

In Fig. 9, each rectifier is made by simply shifting an atomic level out of resonance in the A or the B chains. Introduced in a single tight-binding chain, such a shift produces the required asymmetric I-V characteristic of a rectifier[29] as presented in Fig. 9(c). The currents coming from the two rectifying branches are added at the central node of the circuit presented in Fig. 9. The logic levels of the A and B inputs are defined by the voltage applied relative to ground. A 2 V bias provides the "1" logic level and a grounded input the "0" logic level. The output logic levels are defined by the intensity I_C of the tunneling current measured in electrode C using a standard amperemeter. $I_C = 0$ provides the "0" and $I_C \neq 0$ the "1" logic level. The amperemeter is assumed to be interconnected far from the node in the C electrode. In this case, I_C can be calculated using the generalized Buttiker-Landauer formula[30]

$$I_n = \frac{e^2}{\pi\hbar} \int_{-\infty}^{+\infty} \left([1 - \|S_{nn}(E)\|^2] f_n(E) \right. $$

$$\left. - \sum_{j \neq n} \|S_{jn}(E)\|^2 f_j(E) \right) dE, \qquad (19)$$

where $f_l(E) = 1/1 + \exp[(E - \mu_l)/kT]$ is the Fermi-Dirac distribution and μ_l the chemical potential of the electrode l given by $(e - qV_l)$.

The logic behavior of this circuit is presented in Fig. 10. The "0" output logic level is very well defined. But there are
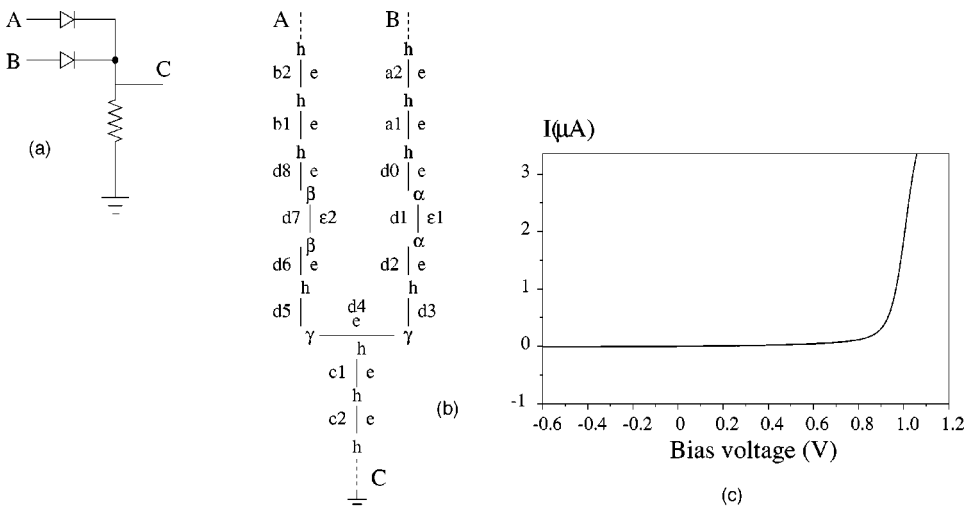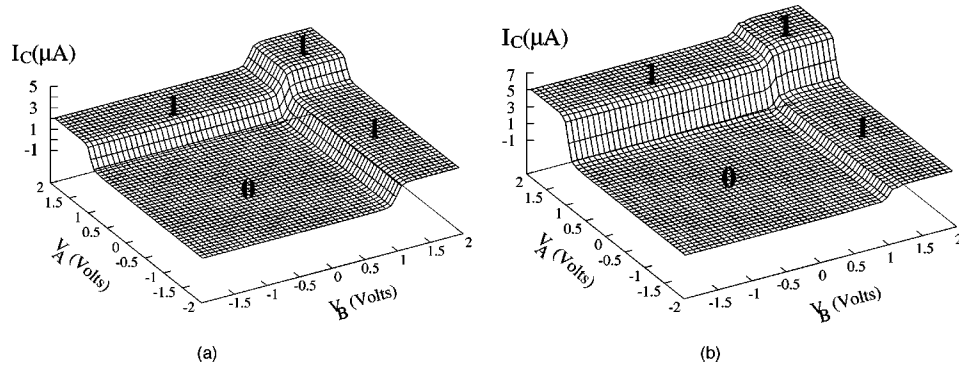

(a)

(b)

(c)

FIG. 9. Design of a "monomolecular" logic OR gate in a ballistic regime. (a) The standard RDL layout of an OR gate with two diodes and one Ohmic resistance R. (b) A ballistic circuit implementation of this OR gate based on two branches with one level out of resonance per branch plus a ballistic three-ports waveguide splitter in the center. (c) The calculated I-V rectifying characteristic of one branch A or B of the circuit.

FIG. 10. The logic response to V_A and V_B input voltage on the logic OR gate (Fig. 9). To reach a large μA output current intensity, $\alpha = 0.1$, $\beta = 0.1$, and $\gamma = 1/\sqrt{2}$ with $\varepsilon_1 = -1$ eV and $\varepsilon_2 = -1$ eV. (a) was calculated with the same number of states per finite length interconnecting chains and (b) with one chain longer by five states than the other one. There are two values of the output current for the high logic level in (a) and three values in (b).

two values of I_C corresponding to the "1" logic level. When the electrodes A and B are biased at 2 V, the output current intensity is twice the value obtained when only one electrode (A or B) is at 2 V and the other is grounded. The usual solution to this problem adopted by the RDL designers was to add an output resistance R in the circuit [Fig. 9(a)]. Introducing such a resistance after the electrode C in the circuit of Fig. 9(b) restores a single "1" output logic level. With such an external resistance, the circuit becomes a hybrid circuit with the resistance in one part and the ballistic three-port node in the other part. One can also emulate this resistance inside the ballistic part by changing, for example, one electronic coupling along the C tight-binding chain (see Sec. IV B). But there is no voltage drop defined along C or between the A and the B branches and the central node (see Sec. IV). This voltage drop is at the basis of a RDL design using R. It is, therefore, not possible in a nonhybrid design to stabilize the same I_C for the three states of the A or B inputs leading to the same "1" output logic state.

The logic response of this circuit is maintained by elongating symmetrically the two chains interconnecting the rectifiers to the central node. But any asymmetric deviation in the electronic structure between these two chains in length, coupling, or energy-level shift will modify the logic response of this circuit. We meet here the well-known sensibility of a ballistic circuit to internal details in composition or dimension already known in microwaves,[31] photonics,[32] and mesoscopic ballistic electron devices.[33] According to the wavelength in use in the ballistic circuit, a precise and very local design is always necessary to avoid, for example, destructive interference effects, which will modify the electrical characteristics of the entire circuit.

IV. THE THREE-PORT CIRCUIT IN A TUNNELING REGIME OF TRANSPORT

To avoid the difficulties met within the ballistic regime of transport in building a monomolecular circuit, the latter can be driven in a tunneling regime. In this case, the electrons are transferred between the electrodes through the circuit. It is the average number of electrons exchanged per second between a given couple of electrodes that gives the tunneling

current intensity I measured by an amperemeter inserted in the macroscopic circuit feeding those two electrodes. Inside the tunnel barrier where the circuit is implanted, the advantage of working in the tunneling regime is that there is no stationary phase defined for a given electron in transit. This results in a simplification of the law of association of molecular branches in parallel with no destructive interference effect in the circuit.[15] The disadvantage of this tunneling regime is that the tunneling current intensity through a molecular circuit decreases exponentially with an increase in the size of the molecular circuit.[34]

To reach a tunneling regime of transport through a molecular wire, the bias voltage applied to this wire has to be much lower than its highest occupied molecular orbital–lowest unoccupied molecular orbital (HOMO-LUMO) gap.[4] To reproduce this condition in the simple three-port circuit of Fig. 3, parts a, b, and c of each of the A, B, and C electrodes have been replaced by finite tight-binding chains with an alternate electronic structure. The tunneling regime in each of the a, b, and c chains is reached for an incident energy of the electrons taken within the HOMO-LUMO gap of these chains. In this simple alternating chain model, the electronic gap width is controlled by the difference $2|h1 - h2|$ between the two alternating electronic couplings $h1$ and $h2$ along the chain.[35] Our final tunnel circuit is made of three chains a, b, and c of 24 states, each interconnecting the A, B, and C electrodes to the central three-port node (Fig. 11).

The full scattering matrix of the circuit presented in Fig. 11 was computed by calculating first the effective energy of the frontier states and the effective coupling through the full three-port node and a, b, and c chains from one of the electrode to the others. Secondly, these energy and couplings wereincluded in Eq. (12) to compute the S matrix elements. The scattering matrix cannot be given analytically for this tunnel circuit because of the complexity of the C matrix in Eq. (8), which is now of order 75.

Figure 12 presents the transmission coefficient from A to B through the full circuit of Fig. 11 as a function of the energy and of the node electronic coupling when $\alpha = \beta = \gamma$. The position of the future band structures for the a, b, and c finite chains are clearly visible together with the HOMO-
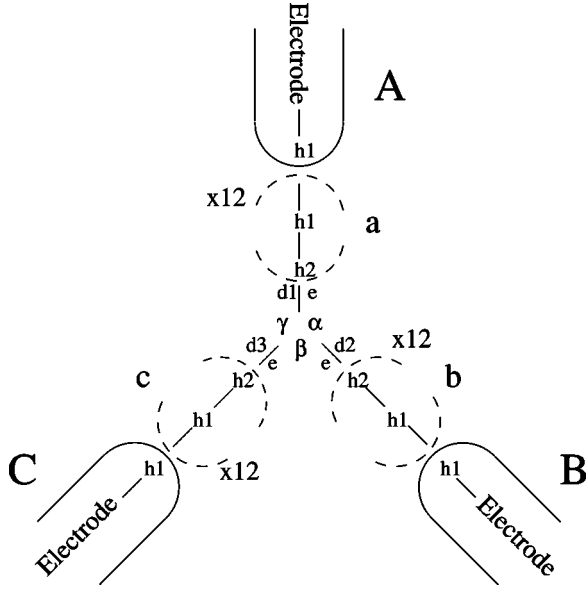
FIG. 11. The tight-binding implementation of a three-port device in tunnel transport regime. The electronic structure of the *A*, *B*, and *C* electrodes is similar to the one in Fig. 3. The finite length 24 states chains *a*, *b*, and *c* link the electrodes *A*, *B*, and *C* to the three central states d_1, d_2, and d_3 of the circuit. Each one of the *a*, *b*, and *c* chains is maintained in a tunneling regime.
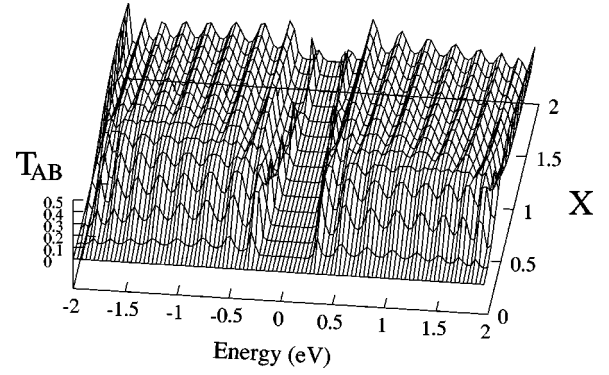

FIG. 12. Transmission coefficient T_{AB} between *A* and *B* through the *a* and *b* tunnel chain and the central node as a function of *X* $= \alpha = \beta = \gamma$ in eV for $h_1 = 1$ eV and $h_2 = 1.2$ eV. The *a* and *b* bandwidth and the central HOMO-LUMO gap depend on the value of *X*.

LUMO gap. The transmission coefficient in the center of this gap is very small and length dependent.

A. The three-port tunnel node

As in the ballistic transport regime discussed in Sec. III, one can search for optimal values of the parameters (α, β, γ) in the circuit of Fig. 11 for which the tunnel current is split in two parts directly inside the tunnel barrier without any access to an intermediate electrode. This tunnel splitter will not be perfect since the reflection coefficient on the input of the circuit will not be zero owing to the choice of a tunnel transport regime. Let us select *A* for the input port of this splitter. The nonzero value of the reflection coefficient R_A has an important consequence: by changing α, β, and γ, the coef-

ficients T_{AB} and T_{AC} can be changed independently because R_A will absorb those changes according to the relation $R_A + T_{AB} + T_{AC} = 1$. This property is different from that of a waveguide splitter in a ballistic transport regime because in this case and when R_A reaches zero, T_{AB} and T_{AC} are related by the condition $T_{AB} + T_{AC} = 1$. In a ballistic regime, the two branches of a waveguide splitter are interdependent because of the conservation of probability. Therefore, in the tunneling regime, the three-port circuit of Fig. 11 cannot be considered as a splitter. This is a "superposer" of tunneling currents. Deep in the tunnel regime, each new branch connected to the central node of Fig. 11 will decrease R_A without changing the transmission properties of the branches already connected on condition that the overall transmission coefficient from *A* to all the other branches is much lower than one.

To illustrate this unique property of a three-port node in the tunnel regime, we have first used our scattering matrix technique to compute R_A, T_{AB}, and T_{AC} of the circuit of Fig. 11, calculating successively R_A and T_{AB} with $\gamma = 0$, R_A and T_{AC} with $\alpha = 0$, and finally R_A, T_{AB}, and T_{AC} with $\alpha = \gamma \neq 0$ while $\beta = 0$ for small α values. As presented in Fig. 13(a), the superposition of the contributions of T_{AB} and T_{AC}
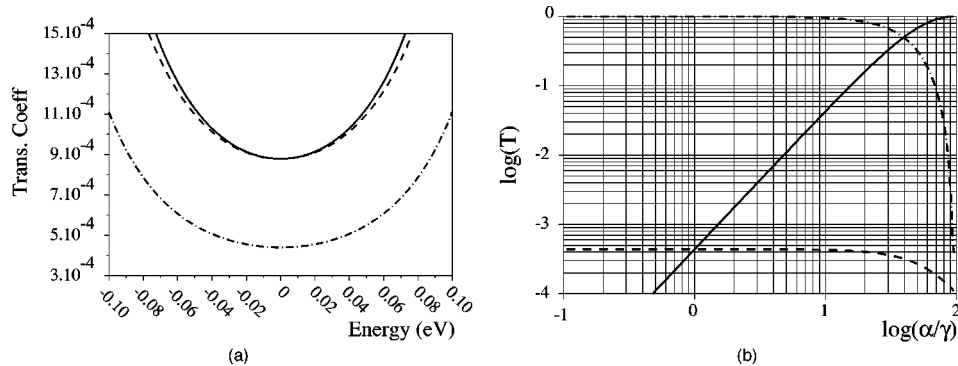

(a)

(b)

FIG. 13. Transmission and reflection coefficient of the Fig. 11 circuit with $\beta = 0$, $e = 0$, $h_1 = 1$ eV, and $h_2 = 1.2$ eV. (a) Solid curve: $1 - R_A$ with $\alpha = \gamma = 1$ eV. Dashed curve: T_{AB} $(\gamma = 0) + T_{AC}$ $(\alpha = 0)$. Dash-dotted curve: T_{AB} $(\gamma = 0, \alpha = 1$ eV$)$ and T_{AC} $(\alpha = 0, \gamma = 1$ eV$)$. (b) Solid and dashed curves: T_{AB} and T_{AC} as a function of α with $\gamma = 1$ eV and $E = 0$. Dash-dotted curve: R_A as a function of α with $\gamma = 1$ eV and $E = 0$.
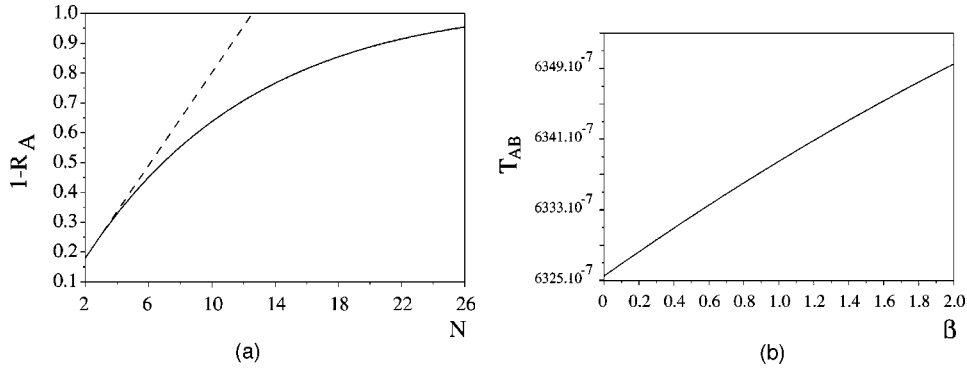
FIG. 14. (a) $(1-R_A)$ plot as a function of the number N of identical output branches in the modified node (Fig. 11) with $\beta=0$, $e=0$, $h_1=1$ eV, $h_2=1.2$ eV, and the electronic coupling linking each electrode to the central level taken to 15 eV. (b) Variation of the transmission coefficient between A and B for the circuit of Fig. 11 as a function of β, with $\alpha=1$ eV, $e=0$, $h_1=1$ eV, and $h_2=1.2$ eV.

occurs with a decrease of R_A while T_{AB} and T_{AC} remain the same as if computed independently. For large α, R_A is so small that T_{AB} increases and saturates. In this regime, T_{AB} and T_{AC} will remain independent if $T_{AC}+T_{AC}$ is very small compared to one. If not, T_{AB} and T_{AC} will be interdependent and the three-port node be almost out of the tunnel regime [Fig. 13(b)].

Notice that for small α values, T_{AB} is proportional to the square of the electronic coupling α, a standard result of the perturbation theory of tunneling.[36] In this case, this coupling α does not compensate for the small effective electronic coupling between A and B through the long alternate a and b chains in series, making this theory applicable to the case of a long chain with a small electronic coupling in its center. For large α values, this small effective coupling is compensated and T_{AB} starts to saturate as a function of α [Fig. 13(b)]. Second, we have calculated R_A while increasing the number of identical branches in the node. R_A decreases as a function of the number N of new branches until it saturates as presented in Fig. 14(a). At this point, the overall transmission from A to all the output branches is maximum and any new branch added to the node will modify the transmission coefficient of all the branches already interconnected.

Deep in the tunnel regime, another consequence of this independence of the branches is that T_{AB} and T_{AC} are independent of β. Therefore and as presented in Fig. 14(b), any change of T_{BC} using β as a tunable parameter will not modify T_{AB} and T_{AC} provided that β is not large enough to saturate T_{BC} to unity. This "rejection" property of a three-port node in a tunnel regime opens the way to the design of an intramolecular transistor.

B. The Kirchhoff laws in the tunnel regime

In the simple electrical circuit of Fig. 15(a), the analytical expression for I_B and I_C are normally obtained using both the well-known "node" and "mesh" Kirchhoff laws. When replacing the Ohmic resistances by tunnel resistances as presented in Fig. 15(c), the analytical expressions for I_B and I_C remain valid. According to the Landauer formula,[37] the dissipation occurs in the electrodes, which means that an electrode-molecular wire-electrode tunnel junction is equivalent to an Ohmic resistance. Here, a tunnel resistance is sim-

ply represented by an alternating electronic tight-binding chain of finite length with a central electronic coupling δ whose value can be tuned as presented in Fig. 15(b) and where the bias voltage must be lower than the electronic gap of the chain. For example, the low-voltage Landauer resistance of this tunnel resistance varies by almost two orders of magnitude from 263 kΩ to 25 MΩ when changing δ from h_1 to $0.1h_1$, respectively, with $h_1=1$ eV.

Instead of substituting only the Ohmic resistances of Fig. 15(a) by tunnel resistances, the complete circuit of Fig. 15(a) including the central three-port node and the wires can be made to work in a tunneling transport regime as proposed in Fig. 15(d). The tight-binding implementation of such a three-port circuit is presented in Fig. 16. This is a simple mono-electronic representation of many of the intramolecular circuits made of a single molecule proposed in the literature.[13,16,38] The interconnection between the three chains is ensured by a three-port symmetric node as discussed in Sec. IV A without passing through a metallic node working, for example, in a diffusive transport regime. The total tunneling current intensity I_A in this circuit can be calculated using the scattering matrix procedure presented in Sec. II with now 75 electronic states composing its tunnel part. The variations of I_A as a function of G_B (with $G_A=G_C$ for simplification) are presented in Fig. 17(a) where I_{A_0} denotes the reference current obtained for $G_A=G_B=G_C$. The values of G_A, G_B, and G_C are given in reference to two electrodes as defined in Fig. 15(b) to make the comparison possible between the Fig. 15(c) and Fig. 15(d) circuits. Inside the tunnel circuit Fig. 15(d), the role of a finite tight-binding chain like G_A, G_B, or G_C is to control the electronic effective coupling between two tunnel wires. When G_B goes to zero, $I_A=0.5I_{A_0}$. Let us now consider each G_A, G_B, and G_C as true tunnel conductances with a well-defined Ohmic conductance when interconnected by standard diffusive metallic wires [Fig. 15(c)]. In this case, I_A can also be calculated using standard electrical circuit rules: when G_B goes to zero, the standard Kirchhoff laws give $I_A=0.75I_{A_0}$.

To understand this difference between the tunnel node of Fig. 15(d) and the diffusive metallic node of Fig. 15(c), we have first computed with our scattering matrix technique the
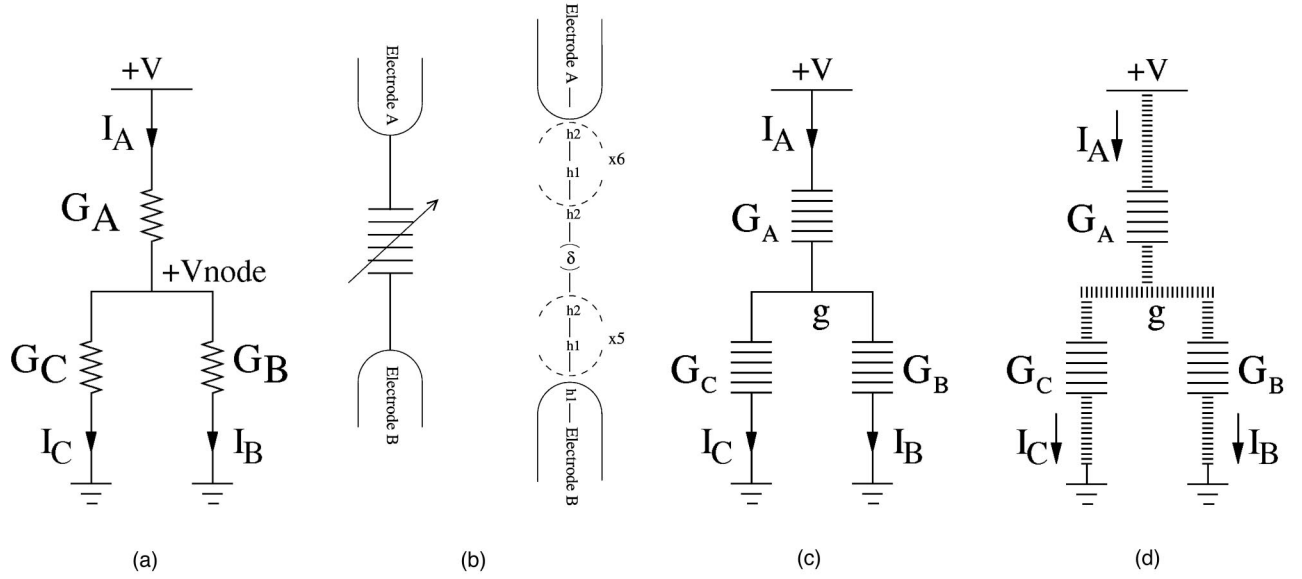
FIG. 15. The same electrical circuit made of one node and three branches with conductance in (a) a diffusive, (c) a tunneling regime of transport, and (d) with the full circuit in a tunnel regime including the node. (b) provides the schematic and the corresponding tight-binding implementation of a tunnel conductance like G_A, G_B, and G_C when they are each connected to two electrodes. In (d), the wire and the conductance are considered in a tunneling regime, meaning that the "conductance" of a given finite length chain is measured by the effective electronic coupling between the two tunnel wires introduced by this chain. It may be better called the "transference" of the chain.

I_B and I_C current intensity in the tunnel circuit of Fig. 16(d). I_C is found to be independent of G_B while I_B is normally controlled by G_B, as presented in Fig. 17(b). In the tunneling regime, this is a consequence of the independence of $T_{AC}(E)$ to a variation of the tunnel parameters controlling the b chain electronic properties as discussed in Sec. IV A. Second, we have verified that the equivalent conductance G of two conductances G_1 and G_2 interconnected in series in a tunnel circuit is $G = (\pi\hbar/e^2)G_1G_2$ (Ref. 15) and not G

$= G_1 G_2/(G_1+G_2)$ as in the standard Ohmic regime, where the two conductances are interconnected in series via a diffusive metallic wire. As a consequence, the variations of I_B and I_C as a function of G_B presented in Fig. 17(b) are quantitatively reproduced by the analytical formula

$$\begin{cases} I_B = (\pi\hbar/e^2)^2 g G_A G_B V, \\ I_C = (\pi\hbar/e^2)^2 g G_A G_C V, \end{cases} \qquad (20)$$
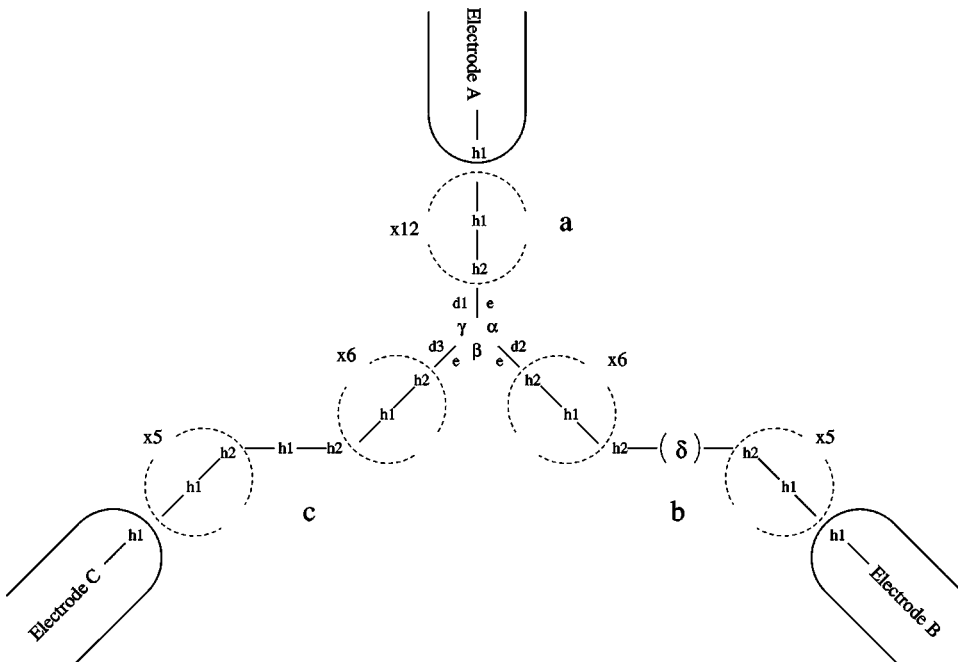

FIG. 16. The detail of the tight-binding version of the Fig. 15(d) circuit with three tunneling chains containing 24 states each.
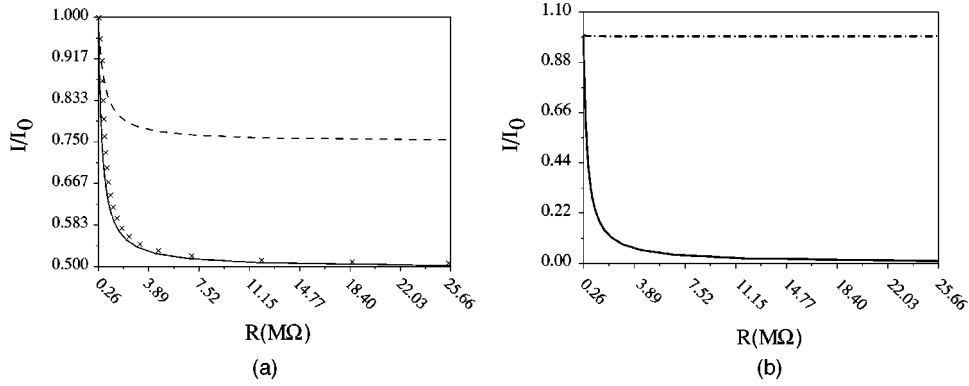
FIG. 17. (a) Comparison of the current intensity I_A as a function of the control resistance R_B in the Boltzmann (dashed curve) and the tunneling (solid curve) regime of transport. The crosses represent the current intensity I_A given by Eq. (21), with $g = 0.2$ μS for the node conductance (Fig. 16). The current intensities are normalized to I_{A_0} obtained for $R_B = R_C$ (or $G_B = G_C$). (b) A representation of the independence in the tunnel regime of the c branch conductance while G_B is modified. Continuous curve for I_B and dash-dotted curve for I_C. For clarity, G_B is represented by R_B. The intensities here are normalized for the $G_B = G_C$ case.

where the conductance g corresponds to the central node tunnel conductance of this three-port tunnel circuit. As presented in Fig. 17(a), it turns out that the total current I_A can also be fitted by a simple superposition of the two analytical expression for I_B and I_C in Eq. (20):

$$I_A = I_B + I_C = \left(\frac{\pi\hbar}{e^2} \right)^2 (gG_AG_B + gG_AG_C)V. \quad (21)$$

This apparent independence of the two branches of a tunnel circuit when G_B goes to zero explains the division by two of I_A in the tunnel circuit of Fig. 15(d) as compared to the factor 3/4 in the case of the standard electronic circuit of Fig. 15(a).

One way to recover intuitively Eq. (21) is to return to the conventional electric circuit "mesh" and "node" Kirchhoff laws. In this case, I_A in the Fig. 15(a) circuit can be decomposed in three terms:

$$I_A = \frac{1}{R_A + R_B}V + \frac{1}{R_A + R_C}V - \left[\frac{R_A}{(R_A + R_B)R_C} \right.$$

$$\left. + \frac{R_A}{(R_A + R_C)R_B} \right] V_{node}. \quad (22)$$

The first two terms in Eq. (22) correspond exactly to the two terms giving I_B and I_C in Eq. (21). They result from the conservation of the electric charge on the central three-port node at the origin of the Kirchhoff node law. The third term in Eq. (22) corresponds to the voltage drop V_{node} occurring at the central node of the circuit in Fig. 15(a). It results from the potential neutrality of a mesh in an electrical circuit and gives rise to the Kirchhoff "mesh" law. In the circuit of Fig. 15(a), V_{node} is a function of the resistances R_A, R_B, and R_C. This is the well-known origin of the interdependence of I_B and I_C on both R_B and R_C. In the tunnel circuit of Fig. 15(d), V_{node} is not physically defined. As a consequence, I_B and I_C are independent. It turns out that this independence reflects in Eq. (22) by simply taking $V_{node} = 0$. In a tunnel circuit, only the "node" Kirchhoff law applies.

C. An OR logic gate in the tunneling regime

As a consequence of the independence of the branches in a circuit driven in a full tunneling regime, the design of an intramolecular logic gate with an RDL architecture will lead to two different output current intensities for the same output high logic level "1" as in the ballistic regime. Furthermore, in the tunnel regime, it is very difficult to stabilize along a tunnel wire an asymmetric resonating state, which will induce a rectification effect in that branch. The reason is that when one level is shifted along an alternating tight-binding chain, this shift has the effect of separating the finite chain into two new shorter chains and the transport regime will remain tunneling. Therefore, those two chains play the role of two effective tunneling barriers for this asymmetric resonant level relative to the electrodes. As a consequence, and for long chains, this resonance will be very sharp and will have no impact on the low voltage I-V characteristic of the full chain. Furthermore, this level must be positioned in the middle of the chain because in the tunnel regime any asymmetry in coupling will sharply attenuate the amplitude of this resonance.

To design our full tunnel OR logic gate, we have chosen to do the reverse: to expel one level from the electronic structure of an alternating finite chain. In this way, a reasonable width is kept for the rectifying resonance and an asymmetric I-V curve is obtained in a chain. We have assembled two such tunnel rectifiers together with a T node, also maintained in a tunnel transport regime as presented in Fig. 18. The full scattering matrix was calculated as indicated in Sec. II for a circuit composed of 143 states in this three-port tunneling barrier. The bias voltage of the input branches was maintained below the HOMO-LUMO gap of the finite chains to drive this gate in a full tunnel regime. The logic levels were defined as in the ballistic case. The logic output current intensity response I_C is presented in Fig. 18(b). As discussed, the "1" logic state of the gate is not well defined. A good point is that the transitions between the "0" and "1" logic state are better defined than in the ballistic case. But this RDL design of an intramolecular logic gate is also much more sensitive to any change or defect in its electronic structure than a ballistic gate.
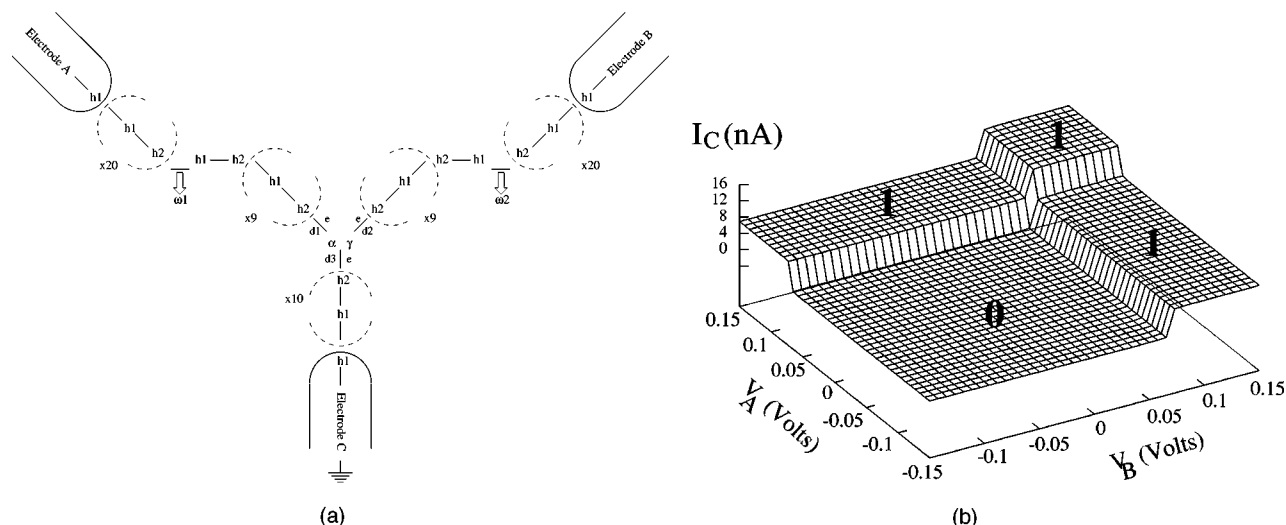
FIG. 18. (a) The tight-binding implementation and (b) the logic response of an OR logic gate working in a full tunnel regime of transport. Input and output logic levels are defined as in Fig. 10 with $\alpha = \gamma = 1$ eV to keep the alternance, h_1 and h_2 values chosen as in Fig. 12. The asymmetric rectifying level are ω_1 and ω_2 with $\omega_1 = \omega_2 = 6$ eV relative to e. I_C was calculated with Eq. (19) after the calculation of the scattering matrix on the full circuit. The input bias voltages V_A and V_B are maintained well below the 0.4 eV HOMO-LUMO gap of the tunnel chains. As a consequence, the output tunneling current intensity is in the nanoampere range.

This very sensitivity points out the need for new architecture concepts in pursuit of the goal of embedding a full logic circuit inside a single molecule as often proposed as the ultimate version of molecular electronics.[3,38] Those new concepts will have to take into account the very fast decrease of the tunnel current intensity in a tunnel circuit with the spatial extension of this circuit.

V. CONCLUSIONS

We have presented a scattering matrix technique for the design of intramolecular circuits connected to N electrodes. This was applied to the study of the electronic transmission and reflection properties of three-port circuits driven in the ballistic or the tunneling transport regime. In particular, we have shown the difficulties of designing a simple OR logic gate in the ballistic regime and demonstrate that only the "node" Kirchhoff law remains valid in the tunneling regime for such a circuit. Our formalism can be used for the description of more complex circuits consisting of a combination of nodes and branches implanted inside the same molecule. This is of importance for the design of complex monomolecular circuits. Of course, the number of circuits that can be designed starting from a combination of single three-port nodes grows rapidly with the number of electrodes interconnecting the circuit to external sources and sinks. Therefore, we have preferred here to present in detail only the properties of the three-port node and its consequences on the design of real circuits. Armed with a tight-binding circuit builder, any circuit topology can be studied using our scattering approach. Furthermore, even through it is restricted to a tight-binding model, our approach provides the background topological and physical properties of any passive circuits embedded inside a single molecule. A more precise calculation of the current intensity in and out of such a circuit requires a detailed molecular-orbital description of each part of the circuit depending on its chemical composition and topology.

[1] A. Dodabalapur, L. Torsi, and H.E. Katz, Science **268**, 270 (1995).
[2] LL. Chuang, L.M.K. Vandersypen, X. Zhou, D.W. Leung, and S. Lloyd, Nature (London) **393**, 143 (1998).
[3] C. Joachim, J.K. Gimzewski, A. Aviram, Nature (London) **408**, 541 (2000).
[4] A. Aviram and M. Ratner, Chem. Phys. Lett. **29**, 277 (1974).
[5] F. Moresco, G. Meyer, K.H. Rieder, H. Tang, A. Gourdon, and C. Joachim, Phys. Rev. Lett. **86**, 672 (2001).
[6] C. Joachim and J.K. Gimzewski, Chem. Phys. Lett. **265**, 353 (1997).
[7] T. Ondarcuhu, C. Joachim, and S. Gerdes, Europhys. Lett. **52**, 178 (2000).
[8] S.J. Tans, R.M. Verschueren, and C. Dekker, Nature (London) **393**, 49 (1998).
[9] V. Derycke, R. Martel, J. Appenzeller, and Ph. Avouris, Nano Letters **1**, 453 (2001).
[10] S. Ami and C. Joachim, Nanotechnology **12**, 44 (2001).

[11] A. Bachtold, P. Hadley, T. Nakanishi, and C. Dekker, Science **294**, 1317 (2001).

[12] Y. Huang, X. Duan, Y. Cui, L.J. Lauhon, K.H. Kim, and C.M. Lieber, Science **294**, 1313 (2001).

[13] F.L. Carter, Physica D **10**, 175 (1984).

[14] V. Langlais *et al.*, Phys. Rev. Lett. **83**, 2809 (1999).

[15] M. Magoga and C. Joachim, Phys. Rev. B **59**, 16 011 (1999).

[16] J.M. Tour, M. Kozaki, and J.M. Seminario, J. Am. Chem. Soc. **120**, 8486 (1998).

[17] P. Sautet and C. Joachim, Phys. Rev. B **38**, 12 238 (1988).

[18] M. Buttiker, Y. Imry, and M.Ya. Azbel, Phys. Rev. A **30**, 1982 (1984).

[19] F. Guinea and J.A. Verges, Phys. Rev. B **35**, 979 (1987).

[20] Z.L. Miskovic, R.A. English, S.G. Davison, and F.O. Goodman, J. Phys.: Condens. Matter **9**, 10 749 (1997).

[21] M. Buttiker, Phys. Rev. Lett. **57**, 1761 (1986).

[22] J.A. Edminister, *Electric Circuits*, 2nd ed. (McGraw-Hill, New York, 1983).

[23] M. Buttiker, IBM J. Res. Dev. **32**, 317 (1988).

[24] M. Buttiker, Phys. Rev. B **32**, 1846 (1985).

[25] T. Itoh, Phys. Rev. B **52**, 1508 (1995).

[26] S.H. Caldwell, *Switching Circuits and Logical Design* (Wiley, New York, 1958).

[27] G. Treboux, P. Lapstun, and K. Silverbrook, Chem. Phys. Lett. **306**, 402 (1999).

[28] Z. Yao, H.W.C. Postma, L. Balents, and C. Dekker, Nature (London) **402**, 273 (1999).

[29] C. Joachim, J.K. Gimzewski, and H. Tang, Phys. Rev. B **58**, 16 407 (1998).

[30] M. Buttiker, Phys. Rev. B **46**, 12 485 (1992).

[31] J. Von Neumann, U.S. Patent No. 2.815.488, Dec. 3 (1957).

[32] R.W. Keyes, Nature (London) **362**, 289 (1993).

[33] R. Landauer, Phys. Today **42** (10), 119 (1989).

[34] M. Magoga and C. Joachim, Phys. Rev. B **56**, 4722 (1997).

[35] M. Magoga and C. Joachim, Phys. Rev. B **57**, 1820 (1998).

[36] T. Gramespacher and M. Buttiker, Phys. Rev. B **56**, 13 026 (1997).

[37] R. Landauer, Z. Phys. B: Condens. Matter **68**, 217 (1987).

[38] J.C. Ellenbogen and J.C. Love, Proc. IEEE **88**, 386 (2000).